Energies **2012**, *5*, 1339-1354; doi:10.3390/en5051339

OPEN ACCESS

energies

ISSN 1996-1073

www.mdpi.com/journal/energies

Article

An Improved Maximum Power Point Tracking Method for Wind Power Systems

Hae Gwang Jeong, Ro Hak Seung and Kyo Beum Lee *

Department of Electrics Engineering, Ajou University, San 5, Woncheon-dong, Yeongtong-gu, Suwon 443-749, Kyunggi-do, Korea; E-Mails: lite88@ajou.ac.kr (H.G.J.); denny3000@ajou.ac.kr (R.H.S.)

* Author to whom correspondence should be addressed; E-Mail: kyl@ajou.ac.kr; Tel.: +82-031-219-2376; Fax: +82-31-212-9531.

Received: 6 April 2012; in revised form: 1 May 2012 / Accepted: 2 May 2012 / Published: 7 May 2012

Abstract: This paper proposes an improved maximum power point tracking (MPPT) method for wind power systems. The proposed method combines hysteresis control with tip speed ratio (TSR) control using a power coefficient curve. It has fast dynamic characteristics with the TSR control using data obtained from an anemometer. Moreover it can track the maximum power point (MPP) with hysteresis control even when there is incomplete data. Since the proposed method selects the operating mode according to the operation state of the generator of three control modes, the controllers do not interfere with each other and they provide excellent performance. The effectiveness of the proposed algorithm is verified by simulation and experiments based on a 3 kW wind turbine system.

Keywords: wind turbine system; MPPT; hysteresis; renewable energy

1. Introduction

Development of renewable energy sources is accelerating due to soaring oil prices and the depletion of fossil fuels [1,2]. Furthermore, the large consumption of conventional fossil energy brings about serious environmental issues such as greenhouse gases, acid rain, and air pollution. Wind turbines generate a low return of energy considering their installation cost, but they have several advantages in terms of higher utilization of land, low pollution and continual use once installed. Small wind power systems are also being actively introduced into cities and parks due to their flexibility of installation [3–5].

As alluded to above, small-sized wind turbines are mostly sited where the energy is needed rather than where the wind quality is best. Cities and parks generally have low and moderate wind speed areas. On the other hand, given Betz's law, wind turbines find it difficult to provide 60% conversion of their input power. They also have some loss factors such as mechanical friction and low efficiency of the generator. Therefore, a maximum power point tracking (MPPT) control method is required to compensate for the low efficiency. There has been an extensive research carried out on approaches to track the maximum power point (MPP) of wind turbines control [6–10].

Generally, MPPT methods can be broadly classified into those that do not use sensors and those that do use sensors. The methods without sensors track the MPP by monitoring the power variation. This method is widely divided into perturbation and observation (P&O) and incremental conductance (IncCond) methods [11,12]. Neither P&O nor IncCond methods require any additional sensors to measure wind or rotor speed, but they have poor dynamic characteristics because they are not usually sensitive to variations in wind speed. Therefore they are mainly used in the small-capacity and low cost systems. The method uses sensors to track the MPP by the control of rotor speed and torque. Basically, it is named the TSR (tip speed ratio) control [13,14]. The TSR control directly regulates the turbine speed or torque to keep the TSR at an optimal value by measuring wind speed and turbine speed [15]. In [16], a fuzzy logic controller is used instead of a typical proportional-integral (PI) controller to control the optimum rotor speed. This algorithm does not require a detailed mathematical model or linearization about an operating point and it is insensitive to system parameter variation. The turbine pitch angle is regulated according to the measured wind speed in [17]. Neural network and fuzzy logic control are applied to improve the performance. An adaptive strategy is shown to improve the performance [18] and its stability is discussed in [19] under conditions that vary the system parameters. In [20], a MPPT method is also using a neural network and Fuzzy Logic for performance improvement. In summary, TSR control offers good performance with fast response and high efficiency. However, an accurate anemometer is expensive and adds extra cost to the system, especially for small-scale systems. Consequently, the TSR control is usually used in huge-capacity systems. In this method, the optimum TSR is dependent on the system characteristics that should be obtained in advance. When it is not possible to obtain accurate data from models of the blade and generator, the problem of not being able to track the MPP occurs. However, there are not solutions to this problem in the previous studies about the TSR control.

The aim of this paper is MPPT control of a 3 kW wind turbine that is installed in a small scale wind farm. This wind turbine has a boost converter for the control of the generator due to its small capacity. It uses TSR control despite its scale, because it operates to connect other wind turbines in the farm. In this paper, a current controller of the boost converter is designed for the MPPT control of this system. In addition, to resolve the previously mentioned problem of using the TSR control, this paper proposes an improved MPPT method. In the proposed MPPT method, the TSR control provides fast dynamic characteristics, and the added hysteresis controller corrects the MPP error at the steady state. The effectiveness of the proposed algorithm is verified by simulation and experiments based on a 3 kW wind turbine system.

2. Controller Design for Wind Power Systems

Figure 1 shows a grid-connected wind power system. The back electromotive force (EMF) of the generator is comprised of a three-phase-sinusoidal voltage that is converted to DC voltage (V_{in}) by a diode rectifier. The MPPT control is performed by adjusting the duty ratio of the DC boost converter on the DC side [13].

Figure 1. Gird-connected wind power systems.

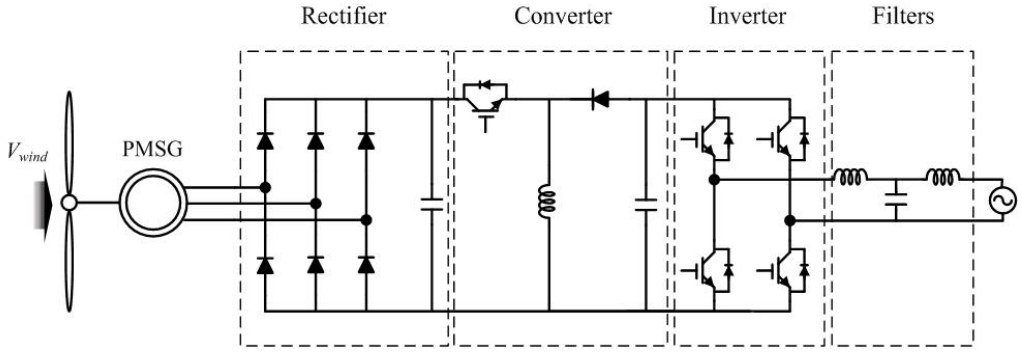

Figure 2 shows the equivalent circuit of the boost converter for the generator control. The boost converter regulates V_{in} by the current or voltage control. The DC-link voltage V_{dc} is controlled by a grid-connected inverter.

Figure 2. Equivalent circuit of the DC-DC converter.

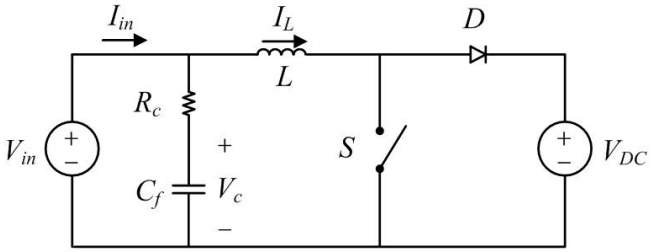

In this figure, L and C_f refer to the filter of the converter and R_c is the equivalent series resistance of the filter capacitor. The state space model can be obtained in order to analyze the nonlinear system. The state vector and input vectors for analysis of the DC-DC circuit are determined from:

$$x = \begin{bmatrix} V_c \\ I_L \end{bmatrix}, \quad u = \begin{bmatrix} V_{DC} \\ I_o \end{bmatrix} \tag{1}$$

The state equation for the voltage and current can be computed using Equation 1, thus:

$$L\frac{dI_L}{dt} = R_C C_f \frac{dV_c}{dt} + V_c \;\Rightarrow\; L\dot{x}_2 = R_c C_f \dot{x}_1 + x_1; \quad I_o = I_L + C\frac{dV_c}{dt} \;\Rightarrow\; I_o = x_2 + C_f \dot{x}_1 \tag{2}$$

If the switch turns on, the state matrix of the circuit is obtained by:

$$\begin{bmatrix} \dot{x}_1 \\ \dot{x}_2 \end{bmatrix} = A_1 \begin{bmatrix} x_1 \\ x_2 \end{bmatrix} + B_1 \begin{bmatrix} V_{DC} \\ I_o \end{bmatrix} \tag{3}$$

where: $A_1 = \begin{bmatrix} 0 & -\frac{1}{C_f} \\ \frac{1}{L} & -\frac{R_c}{L} \end{bmatrix}$, $B_1 = \begin{bmatrix} 0 & \frac{1}{C_f} \\ 0 & \frac{R_c}{L} \end{bmatrix}$.

Moreover, if the switch turns off, the state matrix of the circuit is defined by:

$$\begin{bmatrix} \dot{x}_1 \\ \dot{x}_2 \end{bmatrix} = A_2 \begin{bmatrix} x_1 \\ x_2 \end{bmatrix} + B_2 \begin{bmatrix} V_{DC} \\ I_o \end{bmatrix} \tag{4}$$

where: $A_2 = \begin{bmatrix} 0 & -\frac{1}{C_f} \\ \frac{1}{L} & -\frac{R_c}{L} \end{bmatrix}$, $B_2 = \begin{bmatrix} 0 & \frac{1}{C_f} \\ -\frac{1}{L} & \frac{R_c}{L} \end{bmatrix}$.

Then substituting Equations (3) and (4), the state space of the equivalent circuit can be represented as

$$\dot{\hat{\mathbf{x}}} = A\hat{\mathbf{x}} + B\hat{\mathbf{u}} + [(A_1 - A_2)\mathbf{X} + (B_1 - B_2)\mathbf{U}]\hat{\mathbf{d}} \tag{5}$$

where: $A = \begin{bmatrix} 0 & -\frac{1}{C_f} \\ \frac{1}{L} & -\frac{R_c}{L} \end{bmatrix}$, $B = \begin{bmatrix} 0 & -\frac{1}{C_f} \\ -\frac{D}{L} & -\frac{R_c}{L} \end{bmatrix}$.

Equation (5) can be transformed using Laplace's Equation, and then, the equation is expressed as a state variable:

$$\begin{bmatrix} x_1(s) \\ x_2(s) \end{bmatrix} = \frac{1}{s^2 + \frac{R_c}{L}s + \frac{1}{LC_f}} \begin{bmatrix} s + \frac{R_c}{L} & -\frac{1}{C_f} \\ \frac{1}{L} & s \end{bmatrix} \begin{bmatrix} 0 & \frac{1}{C_f} \\ -\frac{D}{L} & \frac{R_c}{L} \end{bmatrix} \begin{bmatrix} V_{DC}(s) \\ I_o(s) \end{bmatrix} + \frac{1}{s^2 + \frac{R_c}{L}s + \frac{1}{LC_f}} \begin{bmatrix} s + \frac{R_c}{L} & -\frac{1}{C_f} \\ \frac{1}{L} & s \end{bmatrix} \begin{bmatrix} 0 & 0 \\ \frac{1}{L} & 0 \end{bmatrix} \begin{bmatrix} V_{DC}(s) \\ I_o(s) \end{bmatrix} \tag{6}$$

The equation for I_L is then derived from Equation (6) as:

$$\hat{I}_L(s) = \frac{-\frac{Ds}{L}}{s^2 + \frac{R_c}{L}s + \frac{1}{LC_f}} \hat{V}_{DC}(s) + \frac{R_c s}{s^2 + \frac{R_c}{L}s + \frac{1}{LC_f}} \hat{I}_o(s) + \frac{\frac{s}{L}}{s^2 + \frac{R_c}{L}s + \frac{1}{LC_f}} \hat{V}_{DC}(s)\hat{d}(s) \tag{7}$$

Suppose V_{DC} = 0 and ΔV_{DC} = 0, from Equation (7), the transfer function between the inductor current and the duty ratio is presented as

$$v_o = \frac{I_L(s)}{d(s)} = \frac{s}{L} V_{DC} / (s^2 + \frac{R_C}{L}s + \frac{1}{LC_f}) \tag{8}$$

A diagram of the current controller is shown in Figure 3. I_L^* is the reference current to follow the MPP and I_L is the measured current through the boost inductor.

Figure 3. Block diagram of the PI current controller.

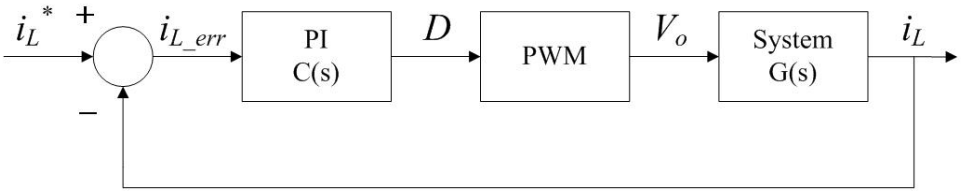

The transfer function of the total system is presented as:

$$T(s) = G(s)C(s) / (1 + G(s)C(s)) \tag{9}$$

where: $G(s) = \frac{s}{L} V_{DC} / (s^2 + \frac{R_c}{L} s + \frac{1}{LC_f})$, $C(s) = \frac{K_P s + K_i}{s}$.

The characteristic equation of a closed-loop transfer function is then used to obtain the system gain, as written below:

$$q(s) = 1 + GC(s) = 1 + K \frac{s}{L} V_{DC} / (s^2 + \frac{R_c}{L} s + \frac{1}{LC_f}) \tag{10}$$

where: $K = \frac{V_{DC}}{L} K_P$.

Figure 4. The root-locus of the current control system.

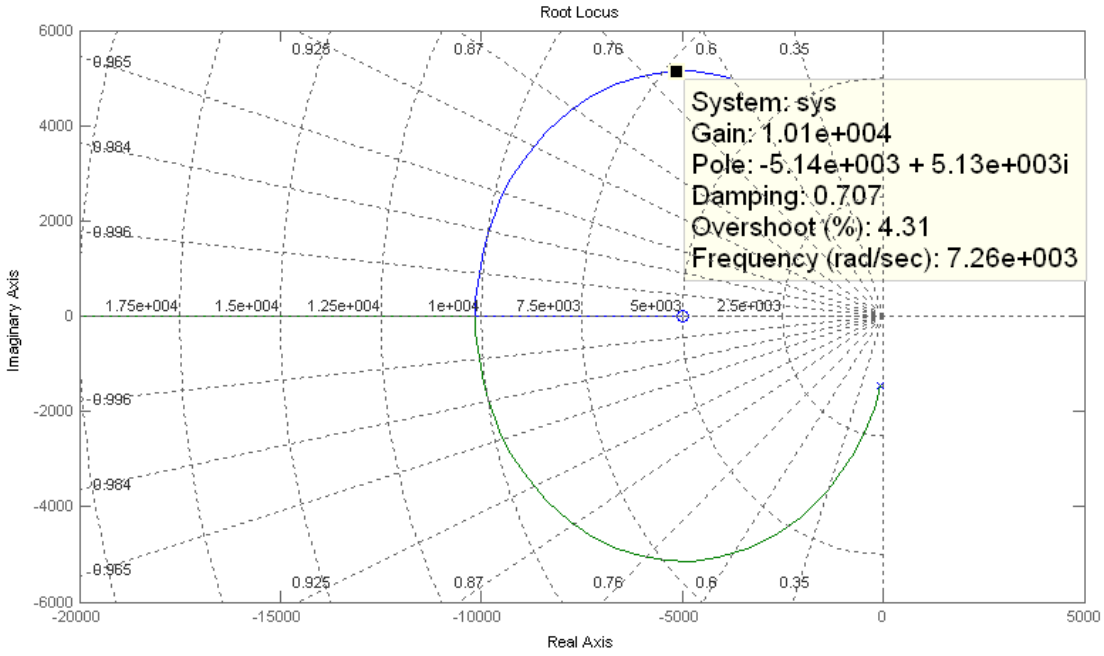

Figure 4 shows the root-locus about Equation (10). If the controller is not sufficiently fast to compensate for the variation in voltage, the ripple of the input voltage can affect the output current. Therefore, for the design of a fast performing controller, the ripple voltage should be considered. System gains are obtained by interpretation of the root-locus. The designed gains of the controller are as follows: PI gains: $K = 10000$, $K_p = 0.0165$, $K_i = 82.5$, $K_a = 60.6$.

3. MPPT Method

3.1. MPPT Method Using TSR *Control*

A wind that passes through the circular area of the turbine blades has an aerodynamic energy that is represented by Equation (11) [11]:

$$P_{wind} = \frac{1}{2} A \rho V_{wind}^3 \tag{11}$$

where A is the circular area of the blade, ρ is the air density, and V_{wind} is the wind speed.

This aerodynamic energy is transformed into kinetic energy depending on the power coefficient (C_p) by blades as:

$$P_{blade} = \frac{1}{2} A \rho V_{wind}^3 C_p(\lambda) \tag{12}$$

The power coefficient is determined by a TSR (λ) and the mechanical conditions, such as the length and pitch angles of the blades. The TSR corresponds to the ratio of the aerodynamic wind energy to the blade kinetic energy, as shown below:

$$\lambda = \frac{\omega_{blade} R_{blade}}{V_{wind}} \tag{13}$$

where ω_{blade} is the angle speed of the blade and R_{blade} is the radius of the blade.

Figure 5. Power coefficient curve.

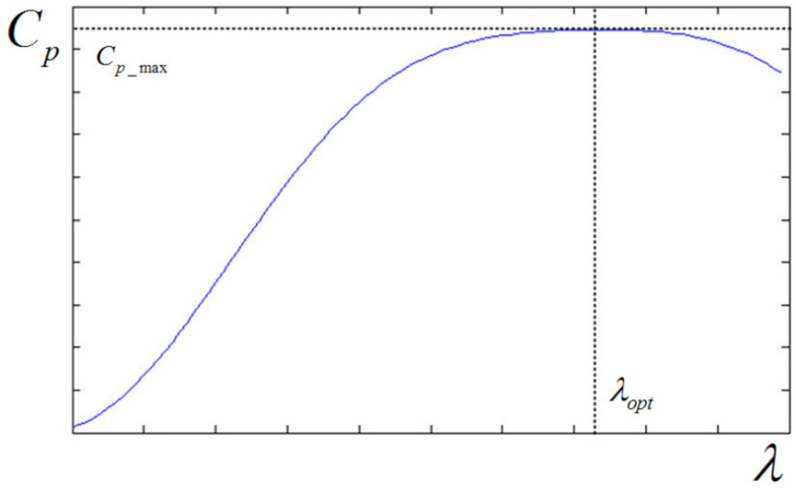

Figure 5 shows the variation of C_p according to the λ. The power coefficient only depends on the TSR. When λ is optimized (λ_{opt}) and C_p becomes a maximum value (C_{p_max}), the kinetic energy gained from the wind is also maximized. The blade torque (T_{blade}) that is delivered to the generator can be calculated by Equation (14) [15]:

$$T_{blade} = \frac{P_{blade}}{\omega_{blade}} \tag{14}$$

In order to generate the maximum power under a variable wind speed, the TSR has to be optimized with variable blade torque. Thus, the reference torque (T_e^*) of the generator is calculated for the MPPT by:

$$K_{blade} = \frac{1}{2} A\rho C_{p\_\max} \left(\frac{R_{blade}}{\lambda_{opt}} \right)^3 ; T_e^* = -(K_{blade}\omega_{blade}^2 - B\omega_{blade}) \tag{15}$$

where K_{blade} and B are a blade constant and a friction coefficient of the revolution system, respectively.

When the generator generates the opposite reference torque to the blade torque, the generated energy is at a maximum value as shown Figure 6.

Figure 6. MPPT control under the variation in wind speed.

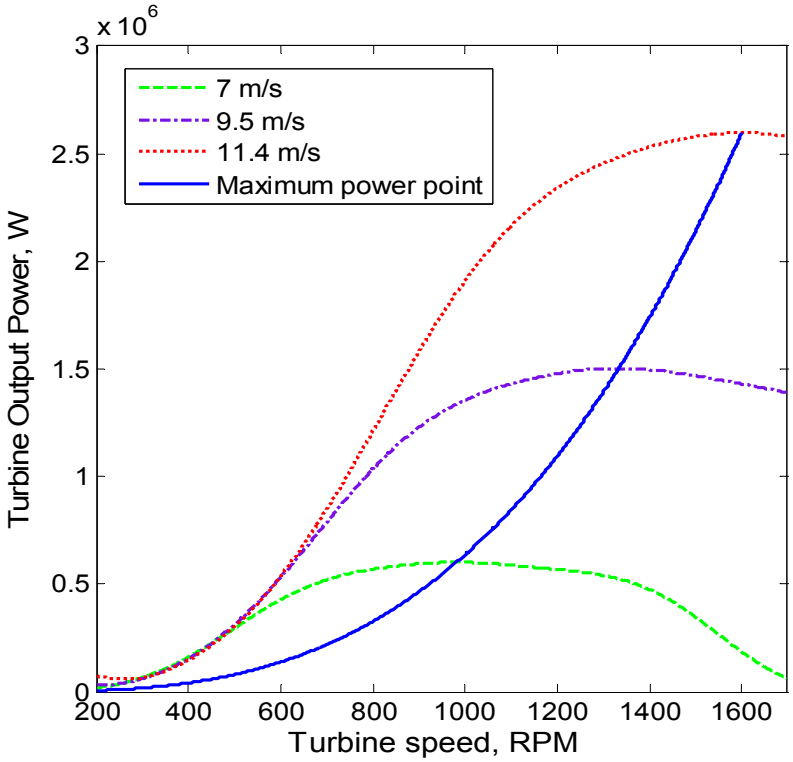

The reference current (i_L^*) of the machine side converter is calculated by:

$$K_t = \frac{3}{4} P\phi_f ; \quad i_L^* = \frac{T_e^*}{K_t} \tag{16}$$

where K_t is a torque constant.

3.2. Proposed MPPT Method with Hysteresis Control

As mentioned previously, an MPPT method using TSR control can rapidly track the MPP. However this MPPT method cannot guarantee the operation of the controller at the MPP when the errors occurring in the C_p-curve are caused by a variance in the blade characteristics. In this paper, the hysteresis controller is combined with TSR control to solve this problem.

Figure 7. The mechanism of hysteresis control.

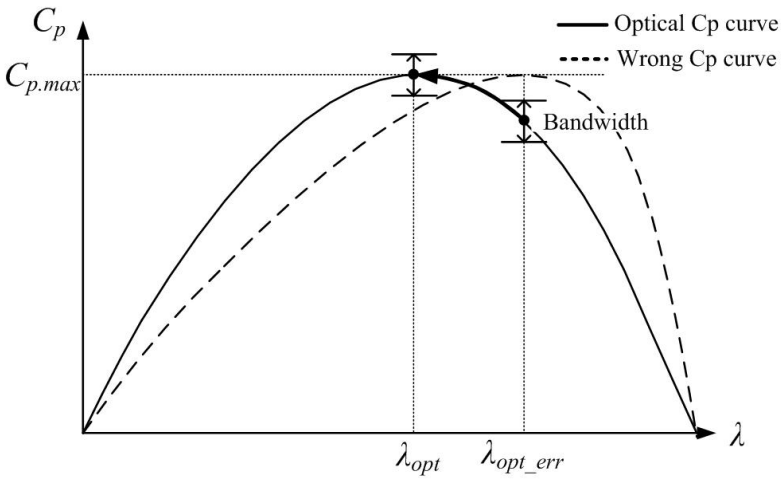

The hysteresis control is similar to that used in the typical P&O control. This controller monitors the power output in order to have a band of maximum power when the wind turbine operates at the MPP of the modeled $C_{p\text{-}curve}$ using TSR control. If the output of the wind turbine is unable to reach maximum power, the hysteresis controller varies the duty ratio within the hysteresis band to correct for the operating point. Figure 7 shows the mechanism by which hysteresis control occurs. The proposed MPPT method includes the following three control modes:

Mode 1: When the changed wind speed makes reference to the current that is derived from the alternative power coefficient curve from that earlier, the controller operates under TSR control mode;

Mode 2: If the change in wind speed, or the error of the TSR controller, is within a certain bandwidth, the controller operates under hysteresis control mode;

Mode 3: If the change in power coefficient is within a certain bandwidth, the controller operates under fixed speed mode.

The control mode is selected by the operating state of the wind turbine. The proposed MPPT method maintains an observation of the variation in wind speed, ΔV_{wind}, and current error variation, ΔI_{err}. When the wind speed changes, ΔV_{wind} is increased. In this situation, the wind turbine is operated under mode 1. If the variation in wind speed is stabilized and ΔV_{wind} meets the established bandwidth, the control mode is determined by ΔI_{err}. When ΔI_{err} is larger than a set value, the controller operates under mode 1. If ΔI_{err} is enough small and the output current follows the reference value, the controller checks whether the power coefficient C_p is set within the band or not. When the C_p value is within the appointed band, the controller is selected to mode 3 and it maintains the operation of the wind turbine. If C_p is not observed to lie within the band, the controller is selected to mode 2 and it corrects the operation of the wind turbine. When C_p reaches a maximum value and the wind turbine operates at the MPP, the controller is set to mode 3.

Figure 8 shows a flowchart for the proposed MPPT method. The output of the previous controller is the feed-forward for the changed mode controller. This feed-forward reduces the disturbance in the power output at the changing point.

Figure 8. Flow chart of the proposed MPPT method.

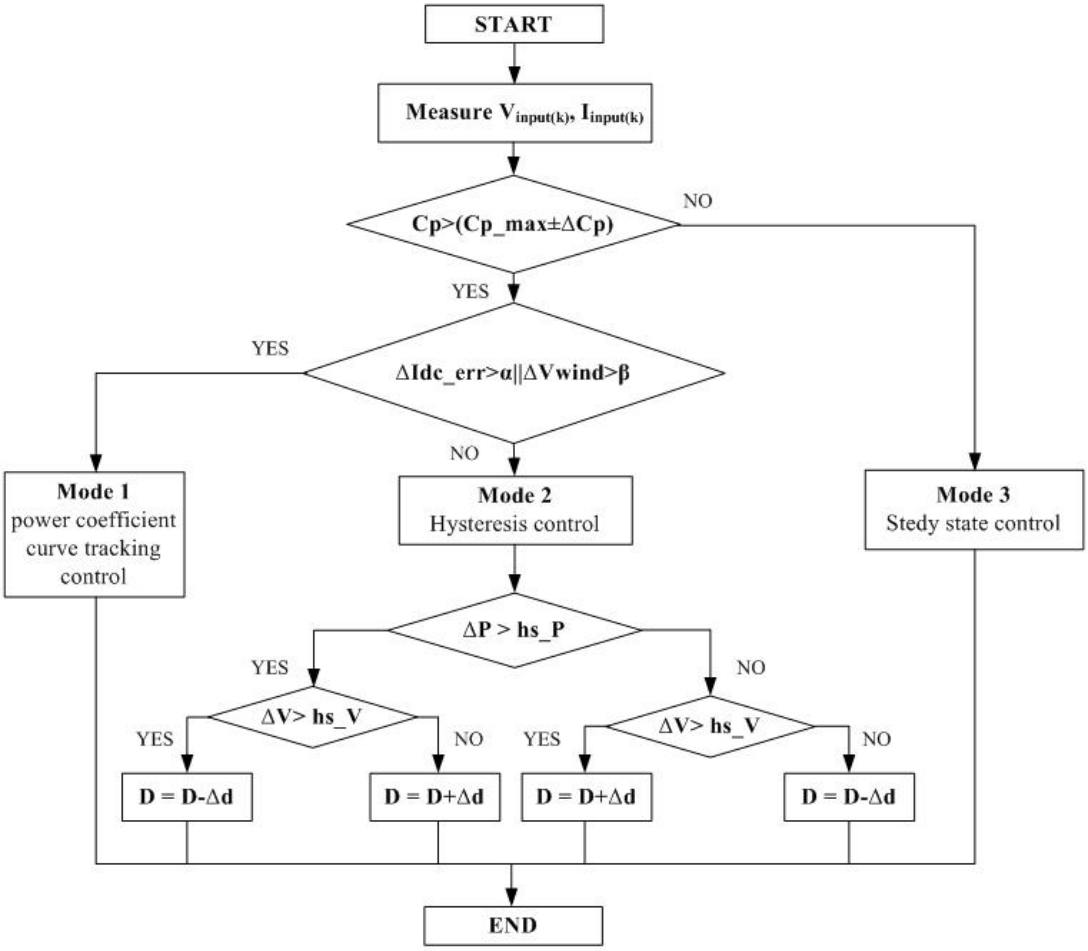

Figure 9 shows the block diagram of the proposed MPPT method. The system normally performs MPPT with the PI-currents control (as shown mode 1 of Figure 8). Then, trigger 1 and 3 are on and trigger 2 is off. When the control mode becomes 2, trigger 1 is off and trigger 2 is on. In this mode, the delta-d of a hysteresis controller is added to the feedback duty ratio (d_{fb}) of the currents controller. This mode is maintained until it is corrected that an error of the duty ratio caused by the mentioned uncorrected model. The duty ratio is fixed to the previous value in mode 3. All of triggers are set to the off position for this operation.

Figure 9. Flow chart of the proposed MPPT method.

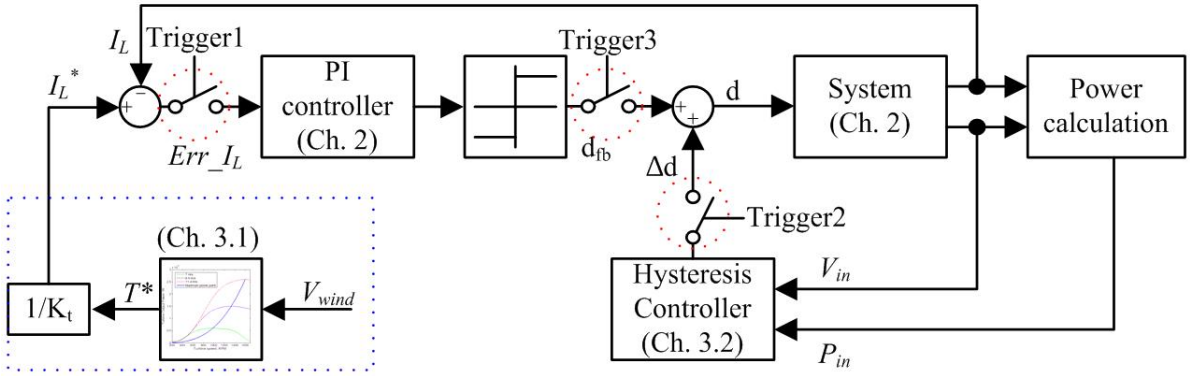

4. Simulations

Simulations were performed using PSIM software to confirm the validity of the proposed MPPT method. The simulation studies were operated for a 3 kW wind turbine model. The simulation parameters related to the small-sized wind turbine system are presented in Table 1.

Table 1. Simulation parameters.

DC-link voltage	400 V
Boost inductance	6 mH
Control period	100 μs
Changes in wind speed	5 to 13 m/s
C_{p_max}	0.475
TSR_{opt}	2.9531

Figure 10 shows the dynamic performance of each controller. For the interval where the wind speed increased from 0.5 to 1.3 s, the P&O method cannot trace the changes in wind speed and C_p drops sharply. On the other hand, the TSR controller can follow C_p by continuously tracking the C_p-curve. The proposed control method operates as mode 1, providing a fast dynamic response to the change in wind speed.

Figure 11 shows the steady-state performance of each controller with uncorrected C_p-curve. In the case of the TSR control method, the power output of the wind turbine follows the wrong C_p-curve. Meanwhile, the P&O method tracks the MPPT because it compares previous power outputs to subsequent power outputs in order to follow the optimal power point. However, the P&O method has a disadvantage in that its operating point swung up and down. The proposed control method operates as modes 2 and 3. When the operating point is corrected, the controller restrains the variation in duty ratio so as to obtain a stable operating point.

Figure 10. Comparison of dynamic performance with each MPPT method.

(**a**) TSR control

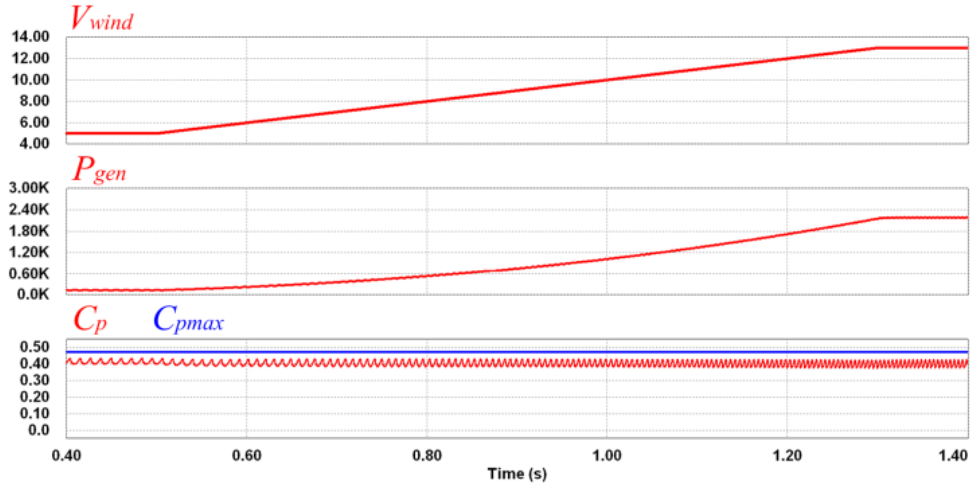

Figure 10. *Cont.*

(**b**) P&O method

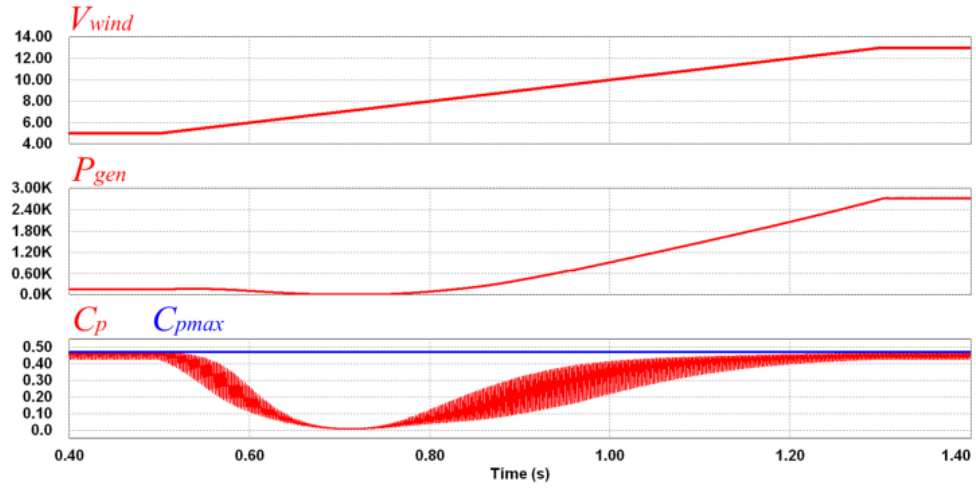

(**c**) Proposed MPPT method

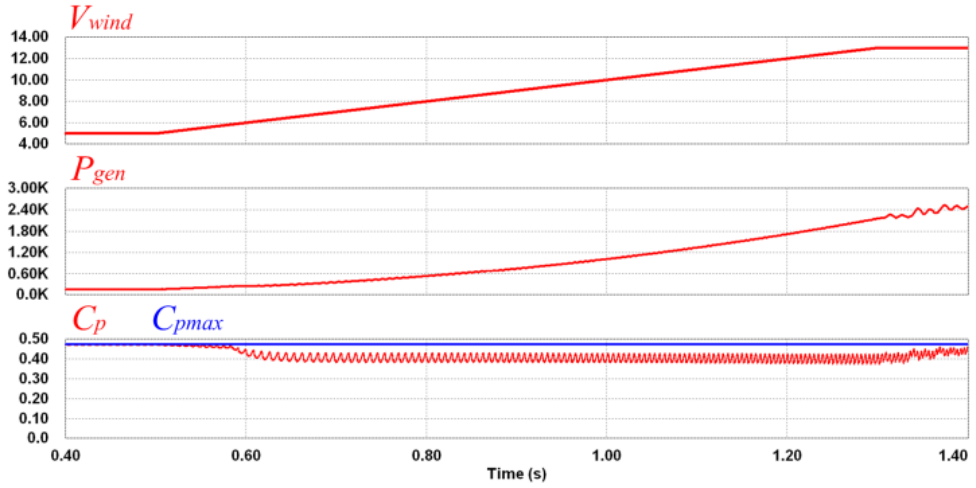

Figure 11. Comparison of steady state performance with each MPPT method.

(**a**) TSR control

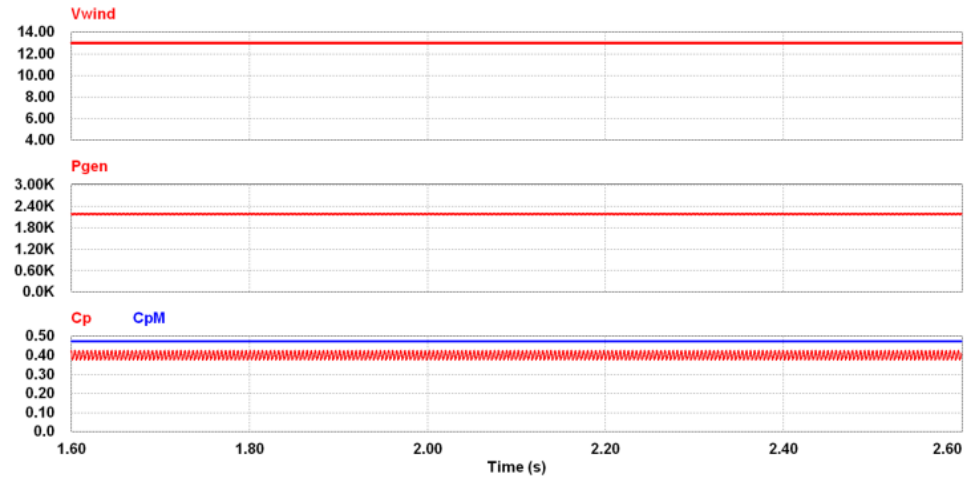

Figure 11. *Cont.*

(**b**) P&O method

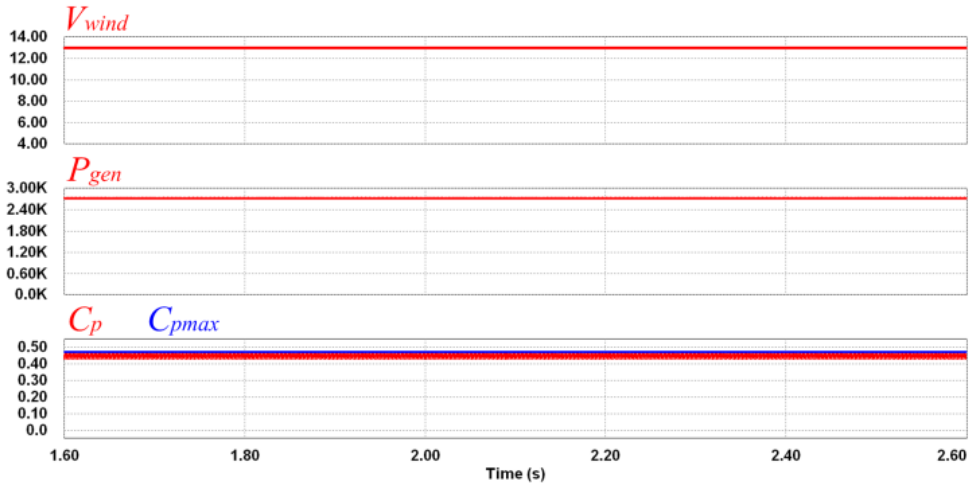

(**c**) Proposed MPPT method

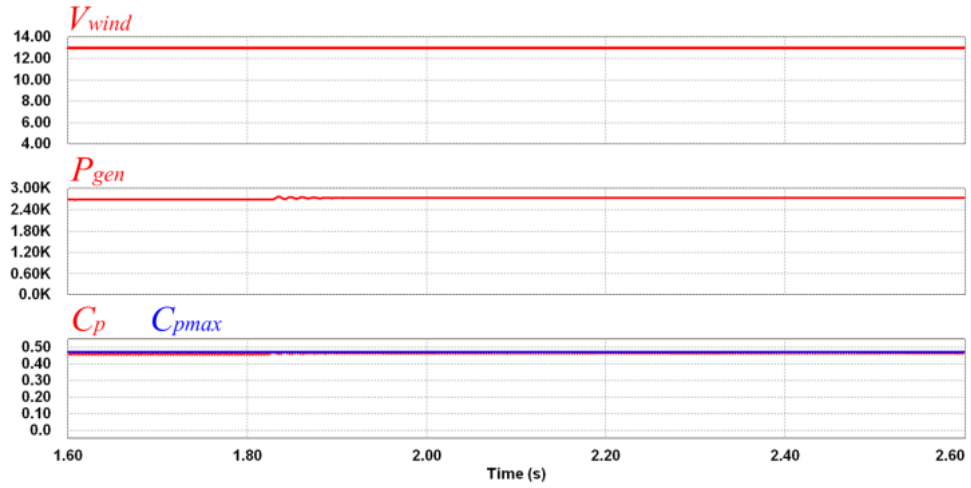

5. Experimental

Figure 12 shows the configuration of the equipment used in the experiments, performed on a 3 kW experimental device operating under the same rated conditions as the simulation studies. The MG-set was used as a model of the wind power generator which formed the basis of the experimental studies to control the speed and torque of the 3 kW, 24 pole synchronous machine with a 15 kW, 380 V, 1740 rpm 4 pole induction machine. The part of power conversion has 10 kHz switching frequency, and consists of two IGBT converters having a DC-link capacitor between two IGBT converters. Table 2 shows some parameter values of the experimental setup.

Table 2. Parameters of experimental setup.

Paramerter		Value
Rated power		3 kW
Rated current (grid side)		13.5 A_{rms}
DC-link voltage		350 V_{dc}
Grid voltage		Single phase 220 V_{rms}
Switching frequency		5 kHz
Boost converter	L_1	3 mH
	C_1	1100 μF
LCLfilter	L_2	3.5 mH
	L_3	2.5 mH
	C_2	10 μF

Figure 12. Experimental setup.

(**a**) Block diagram of experimental setup

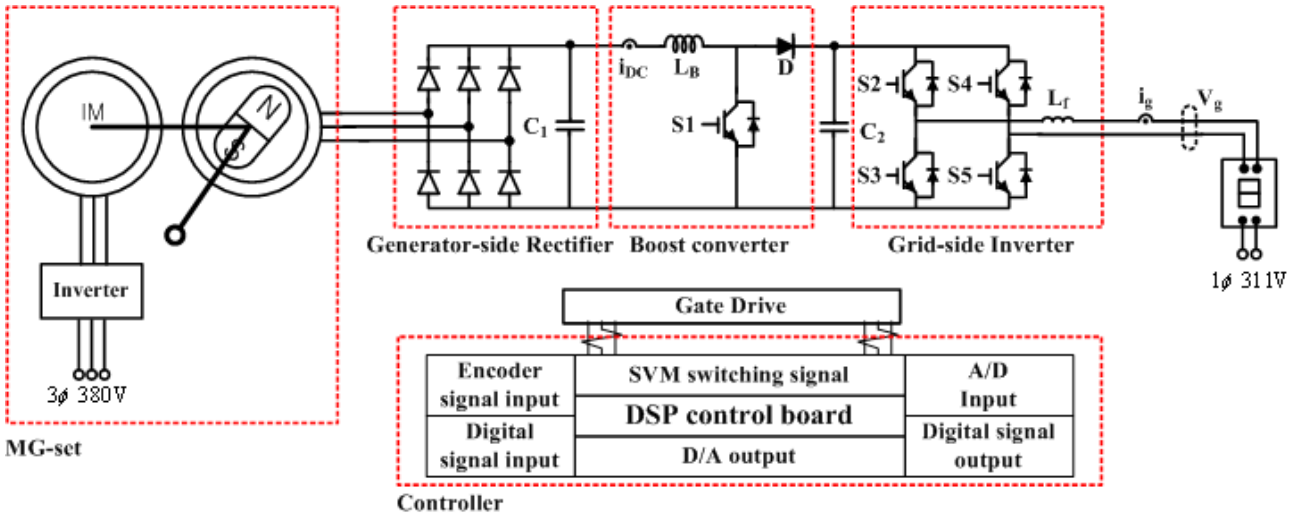

(**b**) MG-set

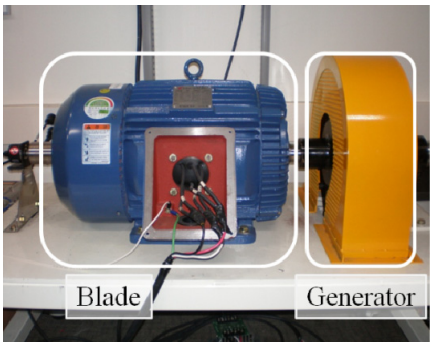

(**c**) Controller

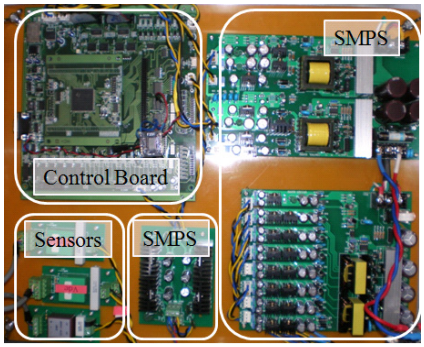

(**d**) Power conversion part

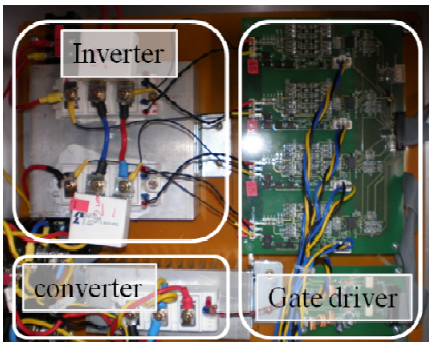

Figure 13. Full operation of the wind power system with the proposed MPPT method.

(**a**) TSR control with corrected C_p curve

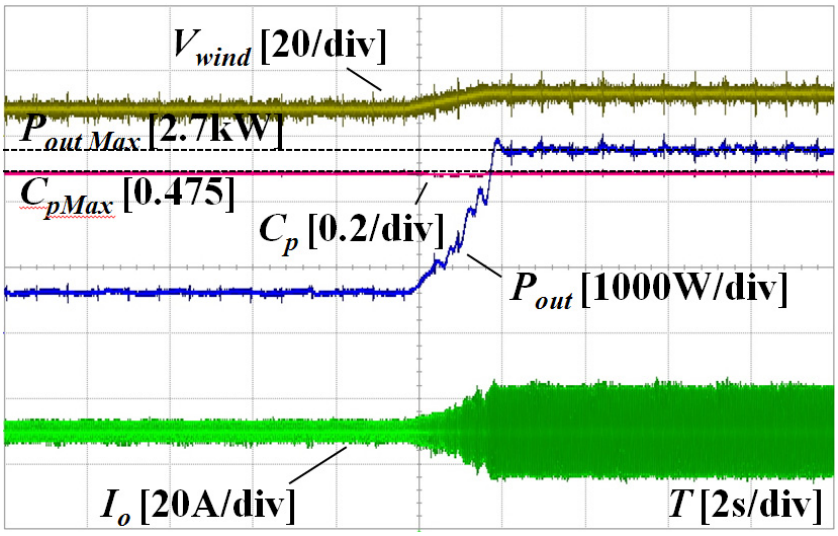

(**b**) TSR control with uncorrected C_p curve

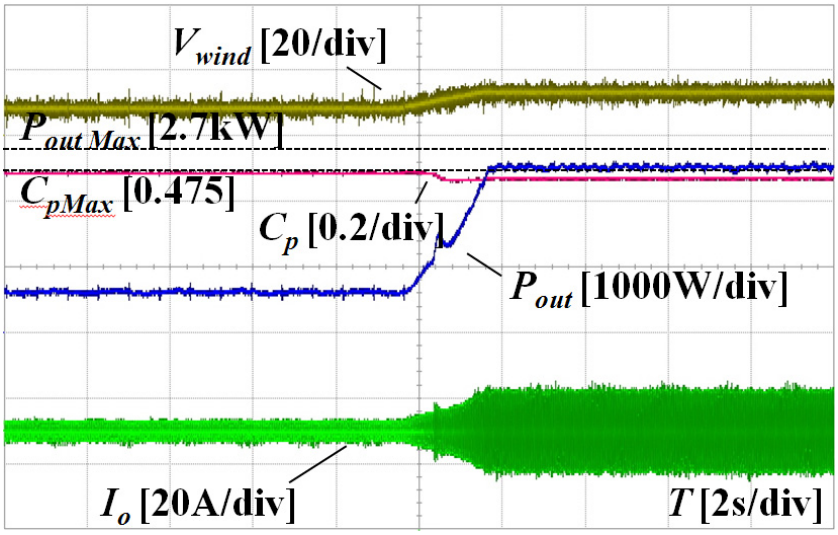

(**c**) Proposed MPPT method

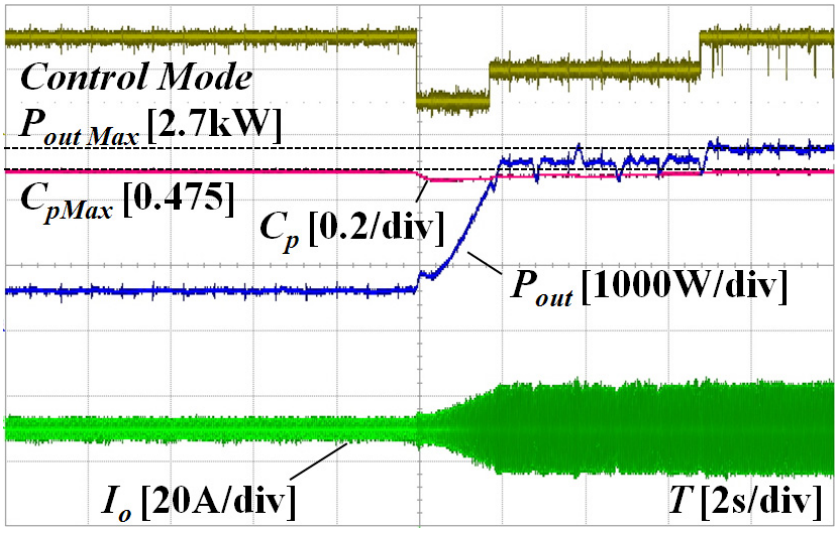

The effectiveness of the proposed MPPT strategy is confirmed in Figure 13. The wind maintained a speed of 8 m/s, before gradually increasing to 13 m/s after 10 s. Figure 13a shows the performance of the typical TSR control with a corrected C_p-curve. It can track the C_{p_max} and the maximum power. However, when the reference current is derived from the uncorrected C_p-curve (14% error of the TSR), the established MPPT method cannot track the maximum power and the C_p is as shown in Figure 13b. Figure 13c shows the performance of our proposed MPPT method. In the region of where the wind speed increased, the controller follows the reference power as mode 1. The wind speed reached to 13 m/s before the controller changed the duty ratio to obtain the correct operating point, as in mode 2. When the C_p arrives at the optimal value, the controller makes the reference duty ratio which is controlled to minimize ripple in power as in mode 3. The interval that wind speed decreases, the controller also repeats the above operation to follow MPP.

This results show that the efficiency of the MPPT is improved about 12% compare with the typical TSR controller. As the error of the parameter is larger than this condition, we can expect excellent effects from the proposed MPPT technique.

6. Conclusions

This paper proposed a MPPT method that combines hysteresis control with TSR control. The proposed control method has fast dynamic characteristics, regardless of changes in wind speed. It also has good steady-state characteristics, where hysteresis control can compensate for current control using a C_p-curve based on incomplete data. In this paper, simulations and experiments were performed on a 3 kW wind power system model.

Acknowledgments

This work was supported by KETEP (20111020400030-11-1-000) which is funded by MKE (Ministry of Knowledge Economy).

References

1. Jeong, H.G.; Lee, K.B.; Choi, S.W.; Choi, W.J. Performance improvement of LCL-filter based grid connected-inverters using PQR power transformations. *IEEE Trans*. *Power Electron*. **2010**, *25*, 1320–1330.
2. Lee, J.S.; Jeong, H.G.; Lee, K.B. Active damping for wind power systems with an LCL filter using a DFT. *J*. *Power Electron*. **2012**, *12*, 326–332.
3. Kortabarria, I.; Andreu, J.; Martinez, D.A.; Ibarra, E.; Robles, E. Maximum power extraction algorithm for a small wind turbine. In *Proceedings of Power Electronics and Motion Control*, Ohrid, Macedonia, 6–8 September 2010; pp. 12–54.
4. Mirecki, A.; Roboam, X.; Richardeau, F. Architecture complexity and energy efficiency of small wind turbines. *IEEE Trans*. *Ind*. *Electron*. **2007**, *54*, 660–670.
5. Chwa, D.K.; Lee, K.B. Variable structure control of the active and reactive powers for a DFIG in wind turbines. *IEEE Trans. Ind. Appl.* **2010**, *46*, 2545–2555.

6. Park, K.W.; Lee, K.B. Hardware simulator development for a 3-parallel grid-connected PMSG wind power system. *J. Power Electron*. **2010**, *10*, 555–562.
7. Kazmi, S.M.R.; Goto, H.; Guo, H.J.; Ichinokura, O. A novel algorithm for fast and efficient speed-sensorless maximum power point tracking in wind energy conversion systems. *IEEE Trans*. *Ind*. *Electron*. **2011**, *58*, 29–36.
8. Pan, T.; Ji, Z.; Jiang, Z. Maximum power point tracking of wind energy conversion systems based on sliding mode extremum seeking control. In *Proceedings of IEEE Energy 2030*, Atlanta, GA, USA, 17–18 November 2008; pp. 1–5.
9. Nguyen, T.H.; Lee, D.C. Improved LVRT capability and power smoothening of DFIG wind turbine systems. *J. Power Electron*. **2011**, *11*, 568–575.
10. Ahmed, T.; Nishida, K.; Nakaoka, M. Wind power grid integration of an IPMSG using a diode rectifier and a simple mppt control for grid-side inverters. *J. Power Electron*. **2010**, *10*, 548–554.
11. Kazmi, S.M.R.; Goto, H.; Guo, H.J.; Ichinokura, O. A novel algorithm for fast and efficient speed-sensorless maximum power point tracking in wind energy conversion systems. *IEEE Trans*. *Ind*. *Electron*. **2011**, *58*, 29–36.
12. Hohm, D.P.; Ropp, M.E. Comparative study of maximum power point tracking algorithms using an experimental, programmable, maximum power point tracking test bed. In *Proceedings of Photovoltaic Specialists*, Anchorage, AK, USA, 15–22 September 2000; pp. 1699–1702.
13. Moor, G.D.; Beukes, H.J. Maximum power point trackers for wind turbines. In *Proceedings of Power Electronics Specialist Conference (PESC)*, Aachen, Germany, 20–15 June 2004; pp. 2044–2049.
14. Nakamura, T.; Morimoto, S.; Sanada, M.; Takeda, Y. Optimum control of IPMSG for wind generation system. In *Proceedings of Power Conversion Conference (PCC)*, Osaka, Japan, 2–5 April 2002; pp. 1435–1440.
15. Tse, K.K.; Ho, B.M.T.; Chung, H.S.-H.; Hui, S.Y.R. A comparative study of maximum-power-point trackers for photovoltaic panels using switching-frequency modulation scheme. *IEEE Trans*. *Ind*. *Electron*. **2004**, *51*, 410–418.
16. Hilloowala, R.M.; Sharaf, A.M. A rule-based fuzzy logic controller for a PWM inverter in a stand alone wind energy conversion scheme. *IEEE Trans*. *Ind*. *Appl*. **1996**, *31*, 57–65.
17. Chedid, R.; Mrad, F.; Basma, M. Intelligent control of class of wind energy conversion systems. *IEEE Trans*. *Energy Convers*. **1999**, *14*, 1597–1604.
18. Johnson, K.; Fingersh, L.; Balas, M.; Pao, L. Methods for increasing region 2 power capture on a variable speed wind turbine. *J. Sol*. *Energy Eng*. **2004**, *126*, 1092–1100.
19. Johnson, K.E.; Pao, L.Y.; Balas, M.J.; Fingersh, L.J. Control of variable-speed wind turbines: Standard and adaptive techniques for maximizing energy capture. *IEEE Trans*. *Control Syst*. *Mag*. **2006**, *26*, 70–81.
20. Jabr, H.M.; Dongyun, L.; Kar, N.C. Design and implementation of neuro-fuzzy vector control for wind-driven doubly-fed induction generator. *IEEE Trans*. *Sustain*. *Energy* **2011**, *2*, 404–414.